ORIGINAL ARTICLE

Structural Synthesis of Parallel Mechanisms with High Rotational Capability

Xiao-Dong Jin, Yue-Fa Fang*, Sheng Guo and Hai-Bo Qu

Abstract

Most parallel mechanisms (PMs) encountered today have a common disadvantage, i.e., their low rotational capability. In order to develop PMs with high rotational capability, a family of novel manipulators with one or two dimensional rotations is proposed. The planar one-rotational one-translational (1R1T) and one-rotational two-translational (1R2T) PMs evolved from the crank-and-rocker mechanism (CRM) are presented by means of Lie group theory. A spatial 2R1T PM and a 2R parallel moving platform with bifurcated large-angle rotations are proposed by orthogonal combination of the RRRR limbs. According to the product principle of the displacement group theory, a hybrid 2R3T mechanism in possession of bifurcated motion is obtained by connecting the 2R parallel moving platform with a parallel part, which is constructed by four 3T1R kinematic chains. The presented manipulators possess high rotational capability. The proposed research enriches the family of spatial mechanisms and the construction method provides an instruction to design more complex mechanisms.

Keywords: Parallel mechanism, Rotational capability, Lie group theory, Bifurcated motion, Hybrid mechanism

1 Introduction

Parallel mechanisms have been extensively researched over many years, depending on their advantages of high speed, high accuracy, large stiffness and heavy-load capability in comparison with the serial counterparts. Such as the famous Delta robot [1], the surgical PMs for medical application [2] and the five-axis machine tools [3]. Several approaches for the structural synthesis of PMs have been proposed. They are the enumeration approach based on the general mobility formula [4, 5], the constraint approach based on the reciprocal screw theory, the synthesis approach based on the Lie group theory [6–8], and the approach based on the theory of linear transformations [9].

However, PMs suffer from the problems of having relatively small useful workspace and limited rotational capability, which are crucial for their performance and applications [10]. It is a more complex process to design PMs with rotational mobility with respect to the translational ones. The classical six Degrees of Freedom (DOF)

PMs often suffer from limited tilting angles due to the joint range limits and the interferences between limbs or between limbs and the moving platform. For example, the famous Stewart platform can only achieve a tilting angle of 40° with respect to the horizontal axis. Hence, the research of PMs with large rotational angles has always been one of the focuses in the structural synthesis of the PMs.

To reach high tilting angles, Kim et al. [11] first proposed the Eclipse with three PPRS (P, R and S denote a prismatic joint, a revolute joint and a spherical joint, respectively) serial limbs for five-face machining in a single setup, which can continuously sweep 360° over the lateral surfaces of the workpiece. Later, the same authors presented a redundantly actuated Eclipse II [12] that can realize continuous 360° rotational motion in any direction and is suitable for the application of flight motion simulators. However, circular guideway makes the translational workspace greatly reduced, which leads to the limited application in need of large translational workspace. Kang et al. [13] developed a 3-DOF micro-positioning PM with 100° tilting angles and analyzed its positioning capability in detail. Using articulated traveling plate to amplify the rotational performance, Pierrot et al. [14–16]

*Correspondence: yffang@bjtu.edu.cn
School of Mechanical, Electronic and Control Engineering, Beijing
Jiaotong University, Beijing 100044, China

Jin *et al. Chin. J. Mech. Eng.* (2018) 31:61

Page 2 of 11

proposed a 4-DOF parallel manipulator known as H-4, which was applied in industrial production. Based on the design of H-4, Krut et al. [17–19] constructed a rotating amplifier using gear sets to develop an I-4 parallel mechanism which can amplify the rotating angles from $\pm 45°$ to $\pm 180°$. A prominent characteristic for the H-4 family is that non-rigid moving platforms are used, after that many PMs with high rotational capability were synthesized utilizing the non-rigid moving platforms. Guo et al. [20, 21] developed a systematic method for the type synthesis of 4-DOF non-overconstrained parallel mechanisms with three translations and one rotation inspired by the H-4 manipulators and presented a class of 4-DOF non-overconstrained parallel mechanisms with large rotational workspace based on screw theory. Wang et al. [22] synthesized a type of 2T3R and 3T3R PMs through constructing different kinds of configurable platforms, which possess high rotational abilities. Oh et al. [23, 24] designed a high maneuverability, high accuracy and large workspace parallel positioning device of which rotational angles can achieve 100°. Liu et al. [25] proposed a family of 3-DOF fully-parallel manipulators which are capable of rotating large angles. Based on the screw theory, Li et al. [26] investigated the identification of the rotational axes of the 3-[P][S] parallel mechanism with different limbs arrangements.

In order to design PMs with large rotational angles, this paper replaces the fixed link of a CRM with additional limbs to obtain a novel PM model based on the relationship between input link and output link of the CRM. On this basis, a series of 1R2T and 1R1T planar PMs are synthesized by means of the Lie group theory. To realize 2-dimension spatial rotations, a 3-RRRR PM and a 4-RRRR parallel moving platform with rotational amplification property and bifurcated rotations are presented. Finally, a hybrid 2R3T mechanism in possession of large rotational angles and bifurcated motion is proposed and analyzed.

The organization of this paper is as follows. In Section 2, a CRM is analyzed and its degenerate model is evolved. Section 3 synthesizes a class of planar 1R1T, 1R2T PMs with large rotational angles and two kinds of spatial PMs with high rotational ability and bifurcated motion by means of the Lie group theory. Using the proposed moving platform, Section 4 constructs a hybrid mechanism, of which mobility and bifurcated property are analyzed. Finally, conclusions are drawn in Section 5.

2 Degenerate CRM Model

The set of six dimensional rigid motion can be endowed with the algebraic structure of a group, represented by D as Lie group [27]. Further any motion of a rigid body can be described by a subset of D, which may be either

a group, called a displacement subgroup (DSG) or a displacement submanifold (DSM) [28, 29]. According to Ref. [30], the 3-dimension subgroup $\{G(\boldsymbol{\mu})\}$ represents 2-dimension translation in a plane and 1-dimension rotation about the normal to the plane. $\{G_2(\boldsymbol{\mu})\}$ denotes 2-dimension displacement manifold, which can be obtained by removal of $\{R(N,\boldsymbol{\mu})\}$ from $\{G(\boldsymbol{\mu})\}$. $\{R(N,\boldsymbol{\mu})\}$ and $\{T(\boldsymbol{\mu})\}$ are the representations of 1-dimension rotational subgroup and translational subgroup, in which $(N, \boldsymbol{\mu})$ represents the axis determined by the unit vector $\boldsymbol{\mu}$ and point N. The displacement set of the end-effector is the product of DSGs of all pairs in a series kinematic chain and the product of groups is closed [31, 32]. Assume that the rigid bodies constructed a limb in a parallel mechanism are 1, 2, 3, ..., $j-1$, j in turn and the DSGs or DSMs (DSGs/DSMs) of the corresponding pairs are $\{D_1\}$, $\{D_2\}$, $\{D_3\}$,..., $\{D_{j-1}\}$, the DSG/DSM of the end of the limb is the product of all the DSGs/DSMs, i.e., $\{L_i\} = \{D_1\}\{D_2\}\{D_3\}\cdots\{D_{j-1}\}$, where $\{L_i\}$ is the DSG/DSM of the end of the limb. The intersection of two subgroups is always a subgroup. The DSG/DSM of the moving platform of a parallel mechanism is the intersection of the DSGs/DSMs of all limbs, i.e.,

$$\{M\} = \bigcap_{i=1}^{n} \{L_i\}, \tag{1}$$

where $\{M\}$ denotes the DSG/DSM of the moving platform and $\{L_i\}$ denotes the DSGs/DSMs of the branches.

As shown in Figure 1, when taking the rocker of a CRM as driving part, the crank outputs whole cycle rotation whereas the rocker swings a certain angle α [33]. This motion principle can be used to construct a rotation amplifying mechanism and be applied to design PMs with large rotational angles.

The planar CRM is constituted by two limbs and a moving platform. Limb 1 is connected by link 1 and link 2 and limb 2 only contains the fixed link 4 and the shortest link 3 is used to be the moving platform. According to the Lie group theory, the DSG of limb
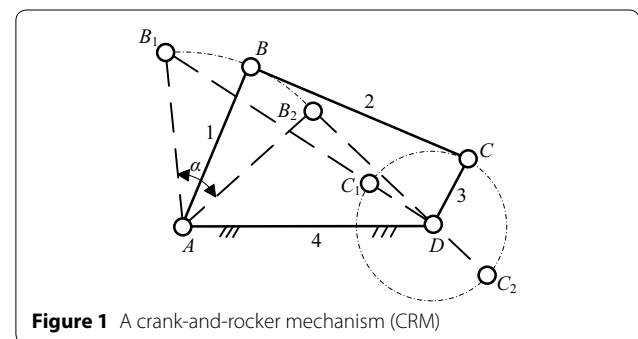

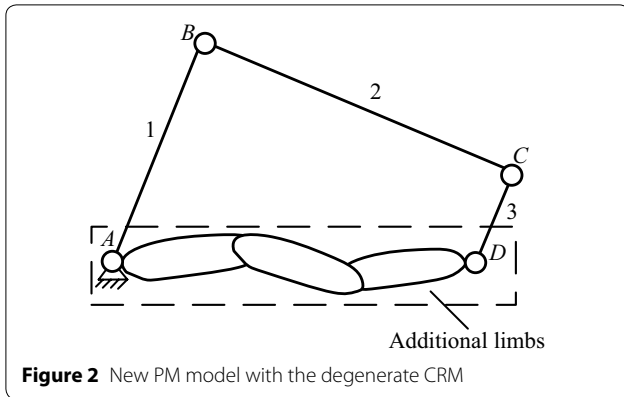**Figure 1** A crank-and-rocker mechanism (CRM)

Jin et al. Chin. J. Mech. Eng. (2018) 31:61

Page 3 of 11

Figure 2 New PM model with the degenerate CRM

Figure 3 Function graph between γ and d

1 can be calculated as $\{R(N_{11}, \boldsymbol{\omega})\}\{R(N_{12}, \boldsymbol{\omega})\}\{R(N_{13}, \boldsymbol{\omega})\} = \{G(\boldsymbol{\omega})\}$, and the DSG of limb 2 is $\{R(N, \boldsymbol{\omega})\}$.

As a result, the DSG of link 3 can be deduced as

$$\{G(\boldsymbol{\omega})\} \cap \{R(N, \boldsymbol{\omega})\} = \{R(N, \boldsymbol{\omega})\}. \tag{2}$$

The above derivation illustrates the motion property of the CRM. If the fixed link 4 is replaced by other limbs to constitute new PMs, as shown in Figure 2, the mobility will be changed and the maximum rotational angle (denoted by γ) of link 3 will be variable due to the distance (denoted by d) between joint A and D is changeable. For brevity and without loss of generality, we let $l_2 > l_1 > l_3$, the relationship between γ and d can be figured as

$$\gamma = \begin{cases} 2\pi - 2\arccos \frac{(d+l_1)^2 + l_3^2 - l_2^2}{2(d+l_1)l_3}, & 0 \leq d < l_2 + l_3 - l_1, \\ 2\pi, & l_2 + l_3 - l_1 \leq d < l_1 + l_2 - l_3, \\ 2\arccos \frac{l_3^2 + d^2 - (l_1 + l_2)^2}{2dl_3}, & l_1 + l_2 - l_3 \leq d \leq l_1 + l_2 + l_3. \end{cases} \tag{3}$$

The function graph is drawn in Figure 3, where the end-effector has a whole cycle rotational ability when d is between $l_2 + l_3 - l_1$ and $l_1 + l_2 - l_3$ and the maximum rotational angle will decrease when d is equal to other values. It is an important guidance for the design of the PMs with large rotational angles.

The kinematic chain connected by link 1, link 2 and link 3 is named as a degenerate CRM. The DSG/DSM of the end-effector in the new PMs can be expressed as

$$\{M\} = \{G(\boldsymbol{\omega})\} \cap \{M_1\}, \tag{4}$$

where $\{M_1\}$ represents the intersection between subsets of the additional limbs,
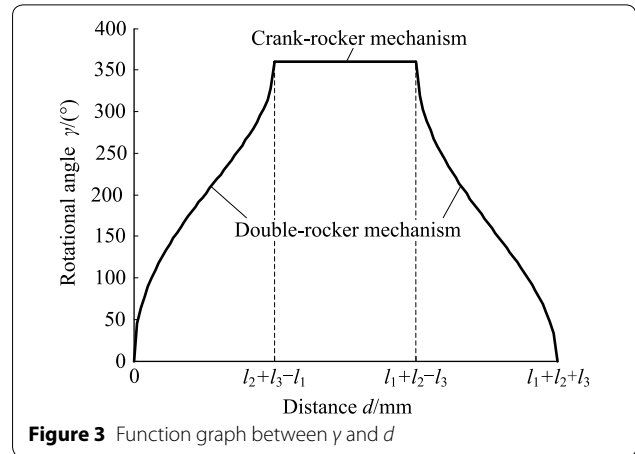
$$\{M_1\} = \bigcap_{i=2}^{n} \{L_i\}. \tag{5}$$

According to Eq. (4), all possible motion the end-effector 3 could output are $\{R(N,\boldsymbol{\omega})\}$, $\{R(N,\boldsymbol{\omega})\}\{T(\boldsymbol{\mu})\}$, $\{R(N,\boldsymbol{\omega})\}\{T(\boldsymbol{\nu})\}$ and $\{G(\boldsymbol{\omega})\}$, which are subsets or proper subsets of $\{G(\boldsymbol{\omega})\}$. Thus, we let the motion types of the additional limbs also be subsets or proper subsets of $\{G(\boldsymbol{\omega})\}$, i.e., $\{M_1\} \subseteq \{G(\boldsymbol{\omega})\}$. A class of planar 1R1T, 1R2T PMs can be synthesized and further a type of spatial 2R1T and 2R PMs can be obtained by appropriate evolution.

3 Structural Synthesis of 1R1T, 1R2T, and 2R1T, 2R PMs

In this section, different limbs are connected with the degenerate CRM to synthesize a series of planar and spatial PMs with large rotational angles in terms of displacement group theory.

3.1 Planar 1R1T and 1R2T PMs
3.1.1 1R1T PMs

Sometimes the rotation center of an end-effector needs to move along a specific line. In other words, the mechanism translates along a line and meanwhile it rotates about any point on this line. For example, the PM could translate along the dasher line k which parallel to x axis in Figure 4(a), or along the dasher line t which parallel to y axis in Figure 4(b), or alone a circle line in Figure 4(c) and rotate with large angles about any point in the given lines.

Therefore, a class of 1R1T PMs is demanded. As known from Lie group theory, $\{R(N_1,\boldsymbol{\omega})\}\{R(N_2,\boldsymbol{\omega})\} = \{R(N,\boldsymbol{\omega})\}\{T(\boldsymbol{\mu})\} = \{G_2(\boldsymbol{\omega})\}$, $\{G_2(\boldsymbol{\omega})\} \cap \{G(\boldsymbol{\omega})\} = \{G_2(\boldsymbol{\omega})\}$, where $\{G_2(\boldsymbol{\omega})\}$ is a subset of $\{G(\boldsymbol{\omega})\}$. Because the DSG of limb 1 is $\{G(\boldsymbol{\omega})\}$, the DSM of the additional limbs must be $\{G_2(\boldsymbol{\omega})\}$ if 1R1T PMs are needed.

For the translation along k parallel to x axis,

Jin *et al. Chin. J. Mech. Eng.* (2018) 31:61

Page 4 of 11
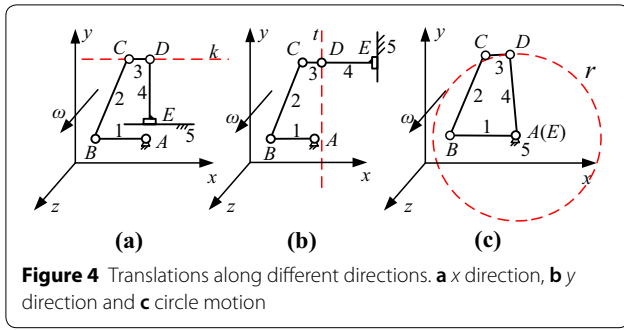
Figure 4 Translations along different directions. **a** *x* direction, **b** *y* direction and **c** circle motion

$$
\begin{aligned}
&\{R(N,\boldsymbol{\omega})\}\{T(\boldsymbol{\mu})\} = \\
&\{G(\boldsymbol{\omega})\} \cap \{R(N,\boldsymbol{\omega})\}\{T(\boldsymbol{\mu})\} = \\
&\{R(N,\boldsymbol{\omega})\}\{T(\boldsymbol{\mu})\}\{T(\boldsymbol{\nu})\} \cap \{R(N,\boldsymbol{\omega})\}\{T(\boldsymbol{\mu})\}.
\end{aligned} \tag{6}
$$

Similarly, for the translation along *t* parallel to *y* axis,

$$
\begin{aligned}
&\{R(N,\boldsymbol{\omega})\}\{T(\boldsymbol{\nu})\} = \\
&\{R(N,\boldsymbol{\omega})\}\{T(\boldsymbol{\mu})\}\{T(\boldsymbol{\nu})\} \cap \{R(N,\boldsymbol{\omega})\}\{T(\boldsymbol{\nu})\}.
\end{aligned} \tag{7}
$$

And for the circular motion along *r*,

$$
\begin{aligned}
&\{R(N,\boldsymbol{\omega})\}\{T(\boldsymbol{r})\} = \\
&\{R(N,\boldsymbol{\omega})\}\{T(\boldsymbol{\mu})\}\{T(\boldsymbol{\nu})\} \cap \{R(N,\boldsymbol{\omega})\}\{T(\boldsymbol{r})\},
\end{aligned} \tag{8}
$$

where vectors $\boldsymbol{\mu}$, $\boldsymbol{\nu}$, $\boldsymbol{\omega}$ represent the orthogonal rotational axes in space which are parallel to *x*, *y*, *z* axes in Cartesian coordinate system respectively. $\{T(\boldsymbol{r})\}$ is perpendicular to link 4 in Figure 4(c) and can be composited by $\{T(\boldsymbol{\mu})\}$ and $\{T(\boldsymbol{\nu})\}$. CAD models of these 1R1T PMs are given as shown in Figure 5. According to Eq. (3) and Figure 3, the rotational angles are variable along with the motion of the prismatic pairs for RRR-RP$_x$ and RRR-RP$_y$ PMs and invariable for RRR-RR PM.

3.1.2 1R2T PMs

Now a class of 1R2T PMs will be synthesized by connecting specific additional limbs with the degenerate CRM. The output DSG of the 1R2T PM is $\{G(\boldsymbol{\omega})\}$ and as

known before, DSG of the degenerate CRM is $\{G(\boldsymbol{\omega})\}$ as well. Hence, DSG of the additional limbs must be $\{G(\boldsymbol{\omega})\}$, without taking the subgroups which are greater than 3-dimension into account.
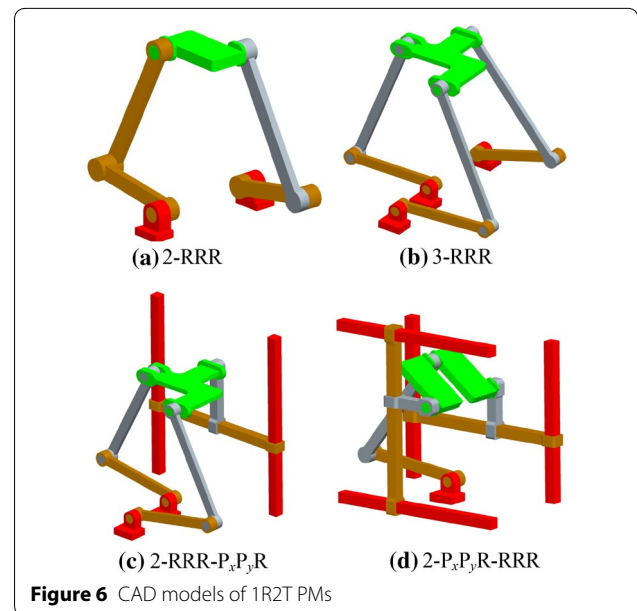
If the new 1R2T PM is connected by two identical limbs, the additional limb is RRR kinematic chain as the first limb and the DSG of the end-effector 3 can be deduced as

$$
\begin{aligned}
&\{R(N_{11},\boldsymbol{\omega})\}\{R(N_{12},\boldsymbol{\omega})\}\{R(N_{13},\boldsymbol{\omega})\}\cap \\
&\{R(N_{21},\boldsymbol{\omega})\}\{R(N_{22},\boldsymbol{\omega})\}\{R(N_{23},\boldsymbol{\omega})\} = \\
&\{G(\boldsymbol{\omega})\}.
\end{aligned} \tag{9}
$$

As a result, a 2-RRR PM can be obtained as shown in Figure 6(a). If two identical limbs which possess the same DSG as the first limb are used as the additional limbs, a 3-RRR PM can be obtained as shown in Figure 6(b). The DSG of the end-effector 3 can be deduced as

$$
\begin{aligned}
&\{R(N_{11},\boldsymbol{\omega})\}\{R(N_{12},\boldsymbol{\omega})\}\{R(N_{13},\boldsymbol{\omega})\}\cap \\
&\{R(N_{21},\boldsymbol{\omega})\}\{R(N_{22},\boldsymbol{\omega})\}\{R(N_{23},\boldsymbol{\omega})\}\cap \\
&\{R(N_{31},\boldsymbol{\omega})\}\{R(N_{32},\boldsymbol{\omega})\}\{R(N_{33},\boldsymbol{\omega})\} = \\
&\{G(\boldsymbol{\omega})\}.
\end{aligned} \tag{10}
$$

The two PMs analyzed above have the same motion properties in view of their DSGs, which both move with two dimensional translations in *xy* plane and one dimensional rotation about axis parallel to *z*. DOF of the two PMs are three, as a result, three actuators are needed for each one. Three actuators can be arranged on the

(a) RRR-RP$_x$ **(b)** RRR-RP$_y$ **(c)** RRR-RR

Figure 5 CAD models of 1R1T PMs

(a) 2-RRR   **(b)** 3-RRR

(c) 2-RRR-P$_x$P$_y$R   **(d)** 2-P$_x$P$_y$R-RRR

Figure 6 CAD models of 1R2T PMs

Jin *et al. Chin. J. Mech. Eng.* (2018) 31:61

Page 5 of 11

base of the three limbs respectively for the 3-RRR PMs. However, one of the two limbs must install two actuators and another limb installs the rest one because there are only two branches for the 3-DOF 2-RRR PMs. It is worth mentioning that the two PMs have whole cycle or close to whole cycle rotational capability based on Figure 3.

$\{G(\boldsymbol{\omega})\}$ can be obtained either by $\{R(N,\boldsymbol{\omega})\}\{T(\boldsymbol{\mu})\}\{T(\boldsymbol{\nu})\}$ or by $\{R(N_1,\boldsymbol{\omega})\}\{R(N_2,\boldsymbol{\omega})\}$ $\{R(N_3,\boldsymbol{\omega})\}$. The PMs indicated by the latter one are presented in Figure 6(a) and Figure 6(b). Now, $\{R(N,\boldsymbol{\omega})\}\{T(\boldsymbol{\mu})\}\{T(\boldsymbol{\nu})\}$ is used to present the additional limbs which are connected in the degenerate CRM in Figure 2. The DSGs of the new PMs are

$$\begin{aligned} &\{R(N_{11},\boldsymbol{\omega})\}\{R(N_{12},\boldsymbol{\omega})\}\{R(N_{13},\boldsymbol{\omega})\}\cap \\ &\{R(N_{21},\boldsymbol{\omega})\}\{R(N_{22},\boldsymbol{\omega})\}\{R(N_{23},\boldsymbol{\omega})\}\cap \\ &\{T(\boldsymbol{\mu})\}\{T(\boldsymbol{\nu})\}\{R(N_3,\boldsymbol{\omega})\} = \\ &\{G(\boldsymbol{\omega})\}, \end{aligned} \tag{11}$$

or

$$\begin{aligned} &\{R(N_{11},\boldsymbol{\omega})\}\{R(N_{12},\boldsymbol{\omega})\}\{R(N_{13},\boldsymbol{\omega})\}\cap \\ &\{T(\boldsymbol{\mu})\}\{T(\boldsymbol{\nu})\}\{R(N_2,\boldsymbol{\omega})\}\cap \\ &\{T(\boldsymbol{\mu})\}\{T(\boldsymbol{\nu})\}\{R(N_3,\boldsymbol{\omega})\} = \\ &\{G(\boldsymbol{\omega})\}. \end{aligned} \tag{12}$$

The additional limbs denoted by $\{T(\boldsymbol{\mu})\}\{T(\boldsymbol{\nu})\}\{R(N,\boldsymbol{\omega})\}$ can be composed by two translational pairs P_xP_y and one revolute pair R, as a result, a 2-RRR-P_xP_yR mechanism and a 2-P_xP_yR-RRR mechanism can be derived as shown in Figure 6(c) and Figure 6(d). Although the 2-RRR-P_xP_yR and 2-P_xP_yR-RRR mechanisms output the same motion as the other two PMs, they have an advantage of restricting the workspace within a specific range through controlling the length of the two translational linkages.

3.2 2R1T and 2R Mechanisms
This part investigates two kinds of mechanisms with large rotational angles whose rotations are not consecutive but bifurcated.

3.2.1 2R1T PM
The novel 3-RRRR PM is presented in Figure 7, where the additional limbs are constituted by two orthogonal arranged RRR limbs. A revolute joint is connected in the end of each limb and its axis is perpendicular to the other revolute joints in this limb in order to provide axes of two directional rotations. Thus, there are four revolute joints for each limb.
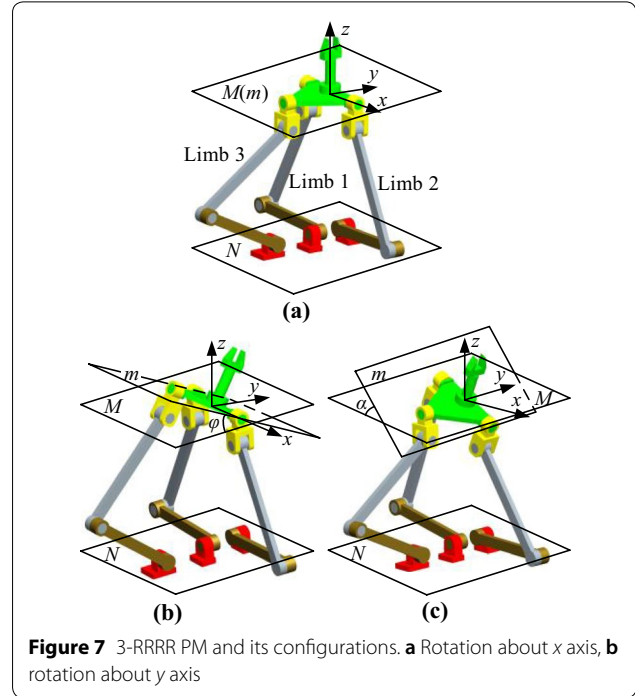
Figure 7 3-RRRR PM and its configurations. **a** Rotation about *x* axis, **b** rotation about *y* axis

We define a reference plane *M* which is always parallel to the base plane represented by *N*. When the plane of the end-effector represented by *m* is parallel to *N*, *M* and *m* are coincided to each other. The DSM/DSG of limb 1 is

$$\begin{aligned} &\{R(N_{11},\boldsymbol{\nu})\}\{R(N_{12},\boldsymbol{\nu})\}\{R(N_{13},\boldsymbol{\nu})\}\{R(N_{14},\boldsymbol{\mu})\} = \\ &\{G(\boldsymbol{\nu})\}\{R(N_{14},\boldsymbol{\mu})\} = \\ &\{T(\boldsymbol{\mu})\}\{T(\boldsymbol{\omega})\}\{R(N_1,\boldsymbol{\nu})\}\{R(N_{14},\boldsymbol{\mu})\}. \end{aligned} \tag{13}$$

Similarly, the DSMs/DSGs of limb 2 and limb 3 are

$$\begin{aligned} &\{T(\boldsymbol{\mu})\}\{T(\boldsymbol{\omega})\}\{R(N_2,\boldsymbol{\nu})\}\{R(N_{24},\boldsymbol{\mu})\}, \\ &\{T(\boldsymbol{\nu})\}\{T(\boldsymbol{\omega})\}\{R(N_3,\boldsymbol{\mu})\}\{R(N_{34},\boldsymbol{\nu})\}. \end{aligned} \tag{14}$$

Thus, the DSM/DSG of the end-effector is

$$\begin{aligned} &\{T(\boldsymbol{\mu})\}\{T(\boldsymbol{\omega})\}\{R(N_1,\boldsymbol{\nu})\}\{R(N_{14},\boldsymbol{\mu})\}\cap \\ &\{T(\boldsymbol{\mu})\}\{T(\boldsymbol{\omega})\}\{R(N_2,\boldsymbol{\nu})\}\{R(N_{24},\boldsymbol{\mu})\}\cap \\ &\{T(\boldsymbol{\nu})\}\{T(\boldsymbol{\omega})\}\{R(N_3,\boldsymbol{\mu})\}\{R(N_{34},\boldsymbol{\nu})\} = \\ &\{T(\boldsymbol{\omega})\}\{R(N,\boldsymbol{\mu})\}\{R(N,\boldsymbol{\nu})\}. \end{aligned} \tag{15}$$

According to the DSM, the end-effector has the motion type of two rotations about *x* and *y* axes and one translation along *z* axis and it is an instantaneous motion only if *m* is parallel to *N*.

When the end-effector rotates a certain angle about *x* axis, shown as Figure 7(b), *m* is no longer parallel to *N* and has an intersection angle ϕ. In other words, the axis

Jin *et al. Chin. J. Mech. Eng.* (2018) 31:61

Page 6 of 11

of the last revolute joint of limb 3 doesn't parallel to any one joint of limb 1 and 2 anymore. The DSMs of limb 1 and 2 remain unchanged, however, the DSM of limb 3 becomes

$$
\begin{aligned}
&\{R(N_{31}, \boldsymbol{\mu})\}\{R(N_{32}, \boldsymbol{\mu})\}\{R(N_{33}, \boldsymbol{\mu})\}\{R(N_{34}, \boldsymbol{t})\} = \\
&\{T(\boldsymbol{v})\}\{T(\boldsymbol{\omega})\}\{R(N_3, \boldsymbol{\mu})\}\{R(N_{34}, \boldsymbol{t})\},
\end{aligned}
\tag{16}
$$

where $\boldsymbol{t}$ denotes the vector of the last joint of limb 3, which is neither parallel nor coincident with y axis.

At this configuration, the DSM of the end-effector is

$$
\begin{aligned}
&\{T(\boldsymbol{\mu})\}\{T(\boldsymbol{\omega})\}\{R(N_1, \boldsymbol{v})\}\{R(N_{14}, \boldsymbol{\mu})\}\cap \\
&\{T(\boldsymbol{\mu})\}\{T(\boldsymbol{\omega})\}\{R(N_2, \boldsymbol{v})\}\{R(N_{24}, \boldsymbol{\mu})\}\cap \\
&\{T(\boldsymbol{v})\}\{T(\boldsymbol{\omega})\}\{R(N_3, \boldsymbol{\mu})\}\{R(N_{34}, \boldsymbol{t})\} = \\
&\{T(\boldsymbol{\omega})\}\{R(N, \boldsymbol{\mu})\}.
\end{aligned}
\tag{17}
$$

Obviously, the end-effector outputs one rotation about x axis and one translation along z axis.

When the end-effector rotates a certain angle about y axis, shown as Figure 7(c), m is no longer parallel to N and has an intersection angle α, and the axes of the last revolute joints of limb 1 and 2 don't parallel to any one joint of limb 3 anymore. The DSM of limb 3 remains unchanged, however, the DSMs of limb 1 and 2 become

$$
\begin{aligned}
&\{T(\boldsymbol{\mu})\}\{T(\boldsymbol{\omega})\}\{R(N_1, \boldsymbol{v})\}\{R(N_{14}, \boldsymbol{k})\}, \\
&\{T(\boldsymbol{\mu})\}\{T(\boldsymbol{\omega})\}\{R(N_2, \boldsymbol{v})\}\{R(N_{24}, \boldsymbol{k})\}.
\end{aligned}
\tag{18}
$$

At this configuration, the DSM of the end-effector is $\{T(\boldsymbol{\omega})\}\{R(N,v)\}$. Hence, the end-effector at this configuration outputs one rotation about y axis and one translation along z axis.

Combining with above analysis, note that there are three bifurcated configurations for the 3-RRRR PM including an instantaneous 2R1T motion only if the end-effector is parallel to the base and the other two 1R1T motions with rotating about x axis and y axis asynchronous as long as the plane of the end-effector intersects with the plane of base.

3.2.2 Rotational Capability Analysis for the 2R1T PM
When the platform rotates about x axis, only one limb controls the rotational angle and the links interference is slight and can be eliminated through reasonable structural design for the platform. Hence, the rotational angle about x axis can reach 360°. However, the platform is controlled by two identical limbs when rotating about y axis, as a result, the interference between these two limbs hampers the whole cycle rotation of the platform. Therefore, it is indispensable to investigate the rotational performance about y axis under the interference model.
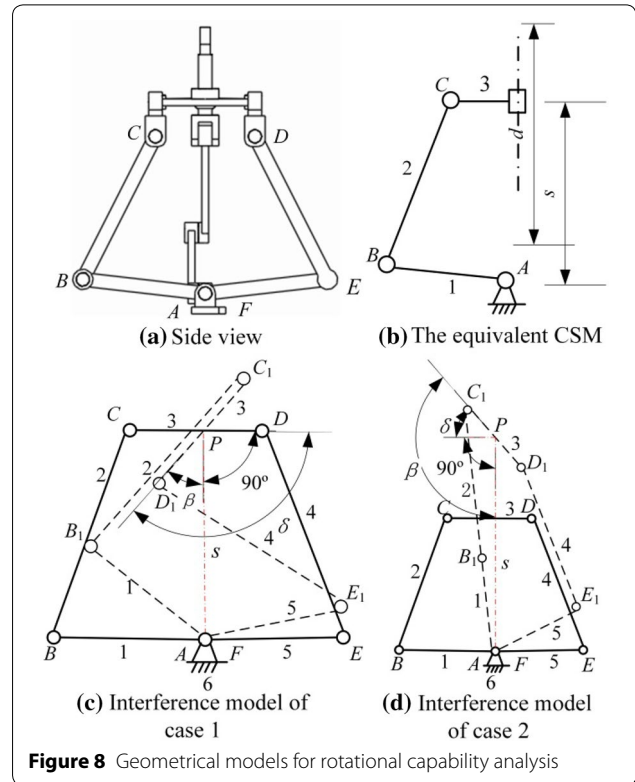

(a) Side view **(b)** The equivalent CSM

(c) Interference model of case 1 **(d)** Interference model of case 2

Figure 8 Geometrical models for rotational capability analysis

From the motion analysis of the 3-RRRR PM, one can find that there is only one translation along z axis if its posture is fixed. This means that the PM can be seen as a crank-slider mechanism (CSM) illustrated in Figure 8(b) at the fixed posture and its translational workspace is equivalent to the slider stroke.
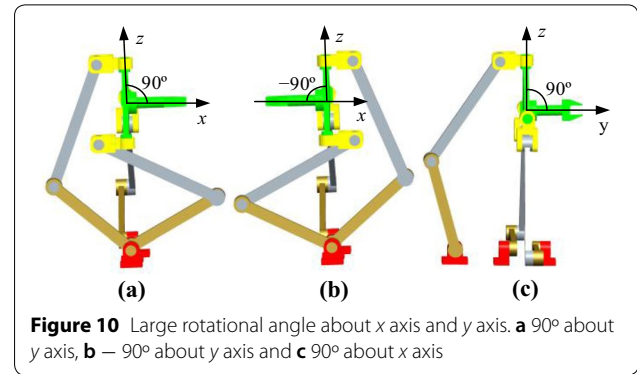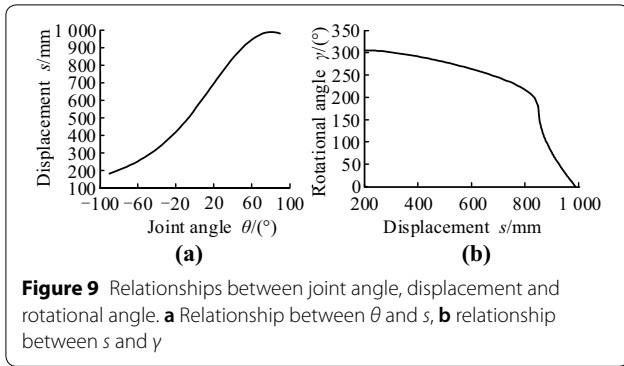
The relationship between the displacement and the input angle associated with joint A can be deduced as

$$
s = l_1 \sin\theta + \sqrt{l_2^2 - (l_1 \cos\theta - l_3/2)^2},
\tag{19}
$$

where s denotes the displacement of the equivalent slider and θ denotes the input angle of the fixed joint A.

The equivalent interference models are shown in Figure 8(c) and Figure 8(d). We assume that the initial posture of end-effector 3 is horizontal and define that the clockwise rotation is positive. There are two kinds of cases that need to be discussed. One is the maximum positive rotational angle is greater than 90° as shown in Figure 8(c) and another is less than 90° as shown in Figure 8(d). These two cases are determined by the displacement s.

In Figure 8(c), when the platform rotates clockwise to closest to coincide with link 2, the end-effector reaches the limit position and can't rotate anymore due to the

Jin *et al. Chin. J. Mech. Eng.* (2018) 31:61

Page 7 of 11

Figure 9 Relationships between joint angle, displacement and rotational angle. **a** Relationship between θ and s, **b** relationship between s and γ

Figure 10 Large rotational angle about x axis and y axis. **a** 90° about y axis, **b** − 90° about y axis and **c** 90° about x axis

interference. In Figure 8(d), the platform can't rotate because it is another limit position, where link 1 and link 2 are collinear. The maximum positive rotational angle can be deduced as

$$\delta = \begin{cases} \beta + 90°, & s_{\min} \le s < s_{90°}, \\ \beta - 90°, & s_{90°} \le s \le s_{\max}, \end{cases} \tag{20}$$

where $s_{\min}$ and $s_{\max}$ denote the minimum and maximum displacements and $s_{90°}$ denotes the displacement value when the maximum positive angle is equal to 90°. β can be figured out in ΔAB_1P in Figure 8(c) and ΔAC_1P in Figure 8(d).

$$\beta = \begin{cases} \arccos \frac{(l_2 - l_3/2)^2 + s^2 - l_1^2}{(2l_2 - l_3)s}, & s_{\min} \le s < s_{90°}, \\ \arccos \frac{s^2 + (l_3/2)^2 - (l_1 + l_2)^2}{sl_3}, & s_{90°} \le s \le s_{\max}. \end{cases} \tag{21}$$

Assume that the length of all links in the equivalent interference model in terms of the 3-RRRR PM in Figure 8(a) is known and let $l_1 = 400$ mm, $l_2 = 600$ mm, $l_3 = 300$ mm. Then the maximum rotational angle γ can be calculated as

$$\gamma = 2\delta. \tag{22}$$

The function curve is drawn under the given size parameters, as illustrated in Figure 9. It should be emphasized that the maximum rotational angle is capable of reaching more than 180° if the displacement is less than $l_1 + l_2 - l_3/2$. In other words, when the translation of the platform makes the values l_1, l_2, l_3 and s conform to the geometrical relationship of a CRM, the PM has the ability of rotating about y axis more than 180°. The maximum rotational angle will drastically decrease when the displacement is greater than $l_1 + l_2 - l_3/2$.

Hence, the manipulator has the ability of rotating about x axis and y axis with large angles. If the end-effector needs to rotate about x axis, it has to move its plane parallel to the base at first and then lock the drives in limb 2 and 3. The similar operation should be taken if the

end-effector needs to rotate about y axis. Figure 10 shows the CAD models about large rotational angles about x axis and y axis respectively.

3.2.3 2R Parallel Moving Platform

On the basis of the above research, a novel symmetric 4-RRRR parallel moving platform with high rotational capability and bifurcated motion is exploited through connecting four 3R kinematic chains orthogonally by a 4R overconstrained close-loop chain. The new parallel moving platform is presented in Figure 11. At the end of each limb the revolute joint whose axis is perpendicular to the other revolute joints in this limb is still needed in order to provide the axes for two directional rotations.

Figure 12 shows the 4R overconstrained close-loop chain in which the axes of revolute joints A, B, C and D are intersected at point O. When the four axes are coplanar, as shown in Figure 12(a), the overconstrained chain is at the singular position where axes of joint A and joint C, axes of joint B and joint D are coincident respectively. It has instantaneous two dimensional rotations about x axis and y axis. When the mechanism rotates a certain angle about joints A and C from the singular position, as shown in Figure 12(b), it remains only one dimensional rotation about y axis because joints B and D can't rotate due to the structural constraints. Similarly, it remains only one dimensional rotation about x axis when the mechanism rotates a certain angle about joints B and D from the singular position as shown in Figure 12(c).

It is worth mentioning that this 4-RRRR PM is used as a parallel moving platform for a hybrid mechanism proposed in the next section, as a result, link A_iB_i ($i = 1$, 2, 3, 4) in each limb is designed that can't rotate about its own axis but be capable of moving with the overconstrained 4R chain and it will be applied mechanical constraints when connected on the hybrid mechanism. Therefore, joint A is not a compound hinge but a single revolute pair. When the PM moves to the configuration

Jin *et al. Chin. J. Mech. Eng.* (2018) 31:61

Page 8 of 11
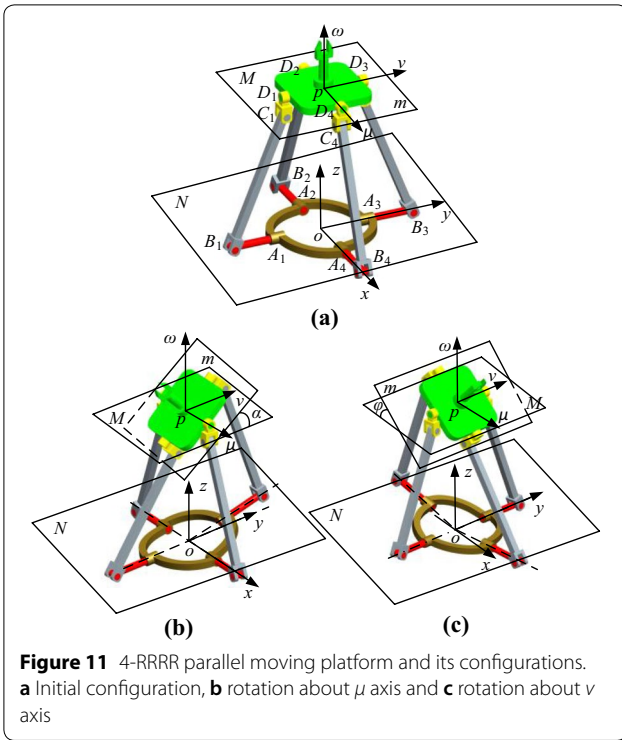
Figure 11 4-RRRR parallel moving platform and its configurations.
a Initial configuration, **b** rotation about *μ* axis and **c** rotation about *v* axis
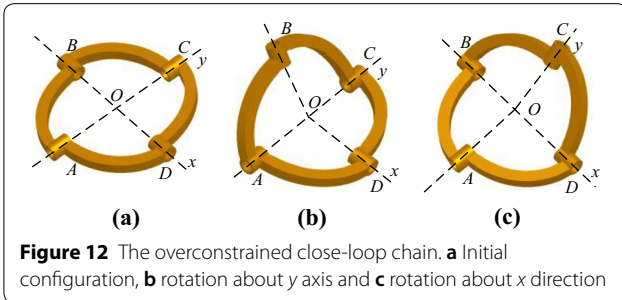
Figure 12 The overconstrained close-loop chain. **a** Initial configuration, **b** rotation about *y* axis and **c** rotation about *x* direction

of plane *m* parallel to plane *N*, as shown in Figure 11(a), the DSM of the four limbs are

Limb1 : $\{R(N_{11}, \boldsymbol{\mu})\}\{R(N_{12}, \boldsymbol{\mu})\}\{R(N_{13}, \boldsymbol{\mu})\}\{R(N_{14}, \boldsymbol{v})\}$,
Limb2 : $\{R(N_{21}, \boldsymbol{v})\}\{R(N_{22}, \boldsymbol{v})\}\{R(N_{23}, \boldsymbol{v})\}\{R(N_{24}, \boldsymbol{\mu})\}$,
Limb3 : $\{R(N_{31}, \boldsymbol{\mu})\}\{R(N_{32}, \boldsymbol{\mu})\}\{R(N_{33}, \boldsymbol{\mu})\}\{R(N_{34}, \boldsymbol{v})\}$,
Limb4 : $\{R(N_{41}, \boldsymbol{v})\}\{R(N_{42}, \boldsymbol{v})\}\{R(N_{43}, \boldsymbol{v})\}\{R(N_{44}, \boldsymbol{\mu})\}$.

It can be found that the Lie group format of each limb is equal to the format of the corresponding limb in the 3-RRRR PM at the reference plane. Consequently, the DSG of the end-effector is also $\{T(\boldsymbol{\omega})\}\{R(N,\boldsymbol{\mu})\}\{R(N,\boldsymbol{v})\}$, which illustrates it has the motion type of two rotations about *μ* and *v* axes and one translation along *ω* axis. The two dimensional rotations are instantaneous DOF at the current configuration. At this singular configuration, axes of joints A_1 and A_3 are coincided and they should be seen as only one revolute pair when calculated by Lie group theory, the same to joints A_2 and A_4.

According to the analysis in Section 2, if joints A_2 and A_4 revolute a smaller angle, the end-effector can output a relatively larger rotational angle *α* as shown in Figure 11(b). At this configuration, the DSMs of the four limbs are

Limb1 : $\{R(N_{11}, \boldsymbol{\mu})\}\{R(N_{12}, \boldsymbol{\mu})\}\{R(N_{13}, \boldsymbol{\mu})\}\{R(N_{14}, \boldsymbol{t})\}$,
Limb2 : $\{R(N_{22}, \boldsymbol{v})\}\{R(N_{23}, \boldsymbol{v})\}\{R(N_{24}, \boldsymbol{\mu})\}$,
Limb3 : $\{R(N_{31}, \boldsymbol{\mu})\}\{R(N_{32}, \boldsymbol{\mu})\}\{R(N_{33}, \boldsymbol{\mu})\}\{R(N_{34}, \boldsymbol{t})\}$,
Limb4 : $\{R(N_{42}, \boldsymbol{v})\}\{R(N_{43}, \boldsymbol{v})\}\{R(N_{44}, \boldsymbol{\mu})\}$.

Thus, the DSM of the end-effector can be deduced as

$$
\begin{aligned}
&\{R(N_{11}, \boldsymbol{\mu})\}\{R(N_{12}, \boldsymbol{\mu})\}\{R(N_{13}, \boldsymbol{\mu})\}\{R(N_{14}, \boldsymbol{t})\}\cap \\
&\{R(N_{22}, \boldsymbol{v})\}\{R(N_{23}, \boldsymbol{v})\}\{R(N_{24}, \boldsymbol{\mu})\}\cap \\
&\{R(N_{31}, \boldsymbol{\mu})\}\{R(N_{32}, \boldsymbol{\mu})\}\{R(N_{33}, \boldsymbol{\mu})\}\{R(N_{34}, \boldsymbol{t})\}\cap \quad (23)\\
&\{R(N_{42}, \boldsymbol{v})\}\{R(N_{43}, \boldsymbol{v})\}\{R(N_{44}, \boldsymbol{\mu})\} = \\
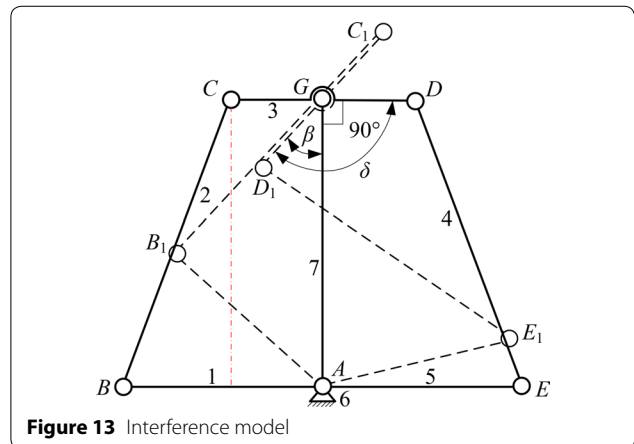&\{R(N, \boldsymbol{\mu})\}.
\end{aligned}
$$

It reveals that the PM only has 1-DOF rotation about *μ* axis at this configuration. Similarly, if joints A_1 and A_3 rotate a smaller angle, the end-effector also outputs a relatively larger rotational angle *φ* and the PM has 1-DOF rotation $\{R(N,\boldsymbol{v})\}$ about *v* axis as shown in Figure 11(c).

3.2.4 Rotational Capability Analysis for the 2R Parallel Moving Platform

The interference model is shown in Figure 13, where the 4-RRRR moving platform can be equivalent to a 2-RRR mechanism in *xz* plane or *yz* plane.

This model can be deemed as a special interference model with a certain displacement value *s* in Figure 8(c). The maximum positive rotational angle is

$$
\delta = \beta + 90^{\circ}, \tag{24}
$$

Figure 13 Interference model

Jin *et al. Chin. J. Mech. Eng.* (2018) 31:61

Page 9 of 11

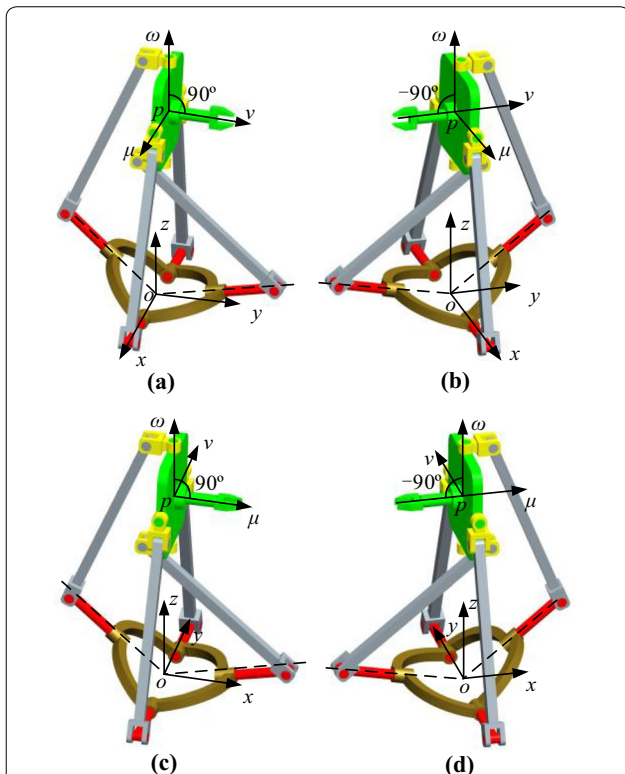where β can be figured out in ΔAB_1G,

$$\beta = \arccos \frac{(l_2 - l_3/2)^2 + s_c^2 - l_1^2}{2(l_2 - l_3/2)s_c}, \tag{25}$$

where s_c denotes the certain displacement value.

$$s_c = \sqrt{l_2^2 - (l_1 - l_3/2)^2}. \tag{26}$$

Equation (24) represents the maximum rotational angle of positive direction. Due to the bifurcation property, this parallel moving platform can rotate about μ axis and ν axis with large angles, both of which range are $\pm\delta$. It is worth mentioning that if the platform would change its rotational direction from one axis to another, it must move to the singular posture at first.

In practical applications, the PMs usually input a given swinging angle θ and the end-effector outputs a larger angle with range of $\pm\delta$. Assuming that the length of all links in the equivalent 2-RRR mechanism in terms of the 4-RRRR PM in Figure 11 is known and still let $l_1 = 400$ mm, $l_2 = 600$ mm, $l_3 = 300$ mm, the maximum positive angle δ can be calculated as $\delta = 136°$ according to Eqs. (24)–(26).
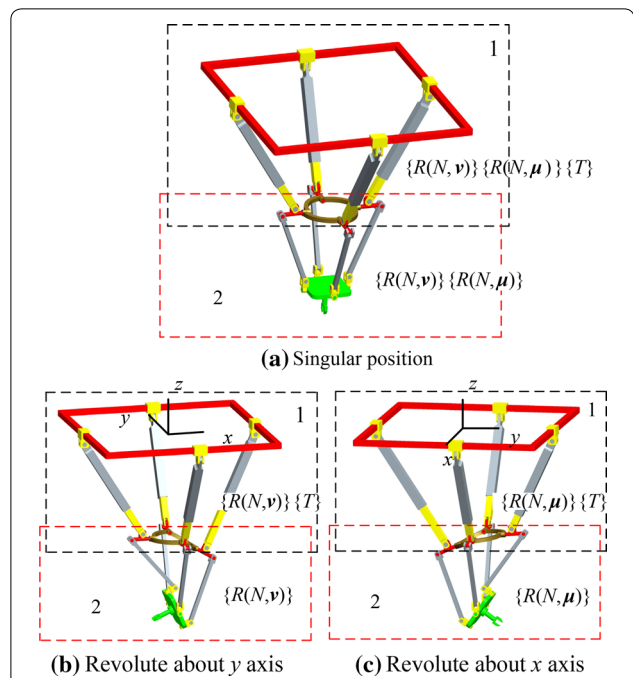
Hence, the rotational range under the given conditions is $\pm 136°$. CAD models with respect to the large rotational angles are demonstrated as Figure 14.

4 2R3T Hybrid Mechanism

The 4-RRRR parallel moving platform is used as a rotating amplifier for the 2R3T hybrid mechanism in this section. As mentioned before, since link A_iB_i in each limb of the 4-RRRR mechanism can't rotate, we let these four links connect with the remaining components of the hybrid mechanism. The DSMs of the hybrid mechanism are $\{R(N,\nu)\}\{R(N,\mu)\}\{T\}$ at singular configuration and $\{R(N,\nu)\}\{T\}$ at one bifurcated configuration and $\{R(N,\mu)\}\{T\}$ at another one. Considering the moving platform only has 1-dimension rotation at either of the two bifurcated configurations and has an instantaneous 2-dimension rotation at the singular posture, it just need to connect the moving platform to a 3T1R parallel component. However, an additional actuator should be installed in one of the four joints of the overconstrained close-loop chain in order to avoid singularity. Since the new component doesn't have moving platform before connecting with the 4-RRRR PM, all limbs are open-loop chains and symmetric distribution and two revolute joints are needed to provide swinging motion about x axis and another two to provide swinging motion about y axis for the parallel moving platform. Therefore, two limbs of

Figure 14 Large rotational angles about μ axis and ν axis. **a** 90° about μ axis, **b** − 90° about μ axis, **c** 90° about ν axis and **d** − 90° about ν axis

(a) Singular position

(b) Revolute about y axis   **(c)** Revolute about x axis

Figure 15 Configurations of the hybrid mechanism

Jin *et al. Chin. J. Mech. Eng.* (2018) 31:61

Page 10 of 11

the 3T1R parallel component associate with the DSM of $\{R(N,\boldsymbol{\mu})\}\{T\}$, however, another two limbs associate with $\{R(N,\boldsymbol{\nu})\}\{T\}$. Since the new parallel component connects with the parallel moving platform in series, the Lie group operation for the two components obeys the product operation.

Hence, a hybrid mechanism with high rotational capability and bifurcated rotations can be derived based on the Lie group analyzed above. The CAD model of this hybrid mechanism is shown in Figure 15.

Now, we will analyze its mobility and bifurcated rotations in another way, however, the large rotational ability will not be demonstrated again which was analyzed before in detail. According to the Lie group theory, the product of two identical DSGs/DSMs is always equivalent to themselves, i.e., $\{R(N,\boldsymbol{\nu})\}\{R(N,\boldsymbol{\nu})\}=\{R(N,\boldsymbol{\nu})\}$. As a result, we divide the hybrid mechanism into two components both of which contain the 4R overconstrained close-loop chain, as the two dashed frames shown in Figure 15.

When the mechanism is at the singular configuration as shown in Figure 15(a), the DSMs associated with all the four limbs in component 1 can be expressed as

$$\{T(\boldsymbol{\mu})\}\{R(N_{11},\boldsymbol{\mu})\}\{T(\boldsymbol{r}_1)\}\{R(N_{12},\boldsymbol{\mu})\}\{R(N_{13},\boldsymbol{\nu})\}\{R(N_{14},\boldsymbol{\mu})\},$$
$$\{T(\boldsymbol{\nu})\}\{R(N_{21},\boldsymbol{\nu})\}\{T(\boldsymbol{r}_2)\}\{R(N_{22},\boldsymbol{\nu})\}\{R(N_{23},\boldsymbol{\mu})\}\{R(N_{24},\boldsymbol{\nu})\},$$
$$\{T(\boldsymbol{\mu})\}\{R(N_{31},\boldsymbol{\mu})\}\{T(\boldsymbol{r}_3)\}\{R(N_{32},\boldsymbol{\mu})\}\{R(N_{33},\boldsymbol{\nu})\}\{R(N_{34},\boldsymbol{\mu})\},$$
$$\{T(\boldsymbol{\nu})\}\{R(N_{41},\boldsymbol{\nu})\}\{T(\boldsymbol{r}_4)\}\{R(N_{42},\boldsymbol{\nu})\}\{R(N_{43},\boldsymbol{\mu})\}\{R(N_{44},\boldsymbol{\nu})\},$$

where $\{T(\boldsymbol{r})\}$ represents the DSG associated with a prismatic pair. The intersection of these four DSMs is equal to $\{R(N,\boldsymbol{\nu})\}\{R(N,\boldsymbol{\mu})\}\{T\}$.

The DSM of the component 2 is already known as $\{R(N,\boldsymbol{\nu})\}\{R(N,\boldsymbol{\mu})\}$ at singular posture. Thus, the DSM of the end-effector can be calculated as

$$\{R(N,\boldsymbol{\nu})\}\{R(N,\boldsymbol{\mu})\}\{T\} \cdot \{R(N,\boldsymbol{\nu})\}\{R(N,\boldsymbol{\mu})\} = \{R(N,\boldsymbol{\nu})\}\{R(N,\boldsymbol{\mu})\}\{T\}. \tag{27}$$

Similarly, the DSMs of the end-effector at two bifurcated configurations can be calculated as

$$\begin{aligned} \{R(N,\boldsymbol{\nu})\}\{T\} \cdot \{R(N,\boldsymbol{\nu})\} &= \{R(N,\boldsymbol{\nu})\}\{T\}, \\ \{R(N,\boldsymbol{\mu})\}\{T\} \cdot \{R(N,\boldsymbol{\mu})\} &= \{R(N,\boldsymbol{\mu})\}\{T\}. \end{aligned} \tag{28}$$

In summary, when the hybrid mechanism moves to the singular configuration, it possesses instantaneous 5-DOF of 3-dimension translations and 2-dimension rotations about x axis and y axis. Nevertheless, when moves to one of the two bifurcated configurations, it possesses 4-DOF of 3-dimension translations and 1-dimension rotation about x axis or y axis. By the way, if the mechanism would move from one configuration to another, it must switch to the singular posture first. Five actuators are needed for

the hybrid mechanism where the four hydraulic cylinders are taken into account and the last one is installed in one of the four joints in the overconstrained close-loop chain.

5 Conclusions

(1) Based on the Lie group theory and the rotational amplifying characteristics of the CRM, a class of planar 1R1T, 1R2T PMs is presented and a spatial 2R1T PM with bifurcated rotations is derived.

(2) A 4-RRRR rotating amplifier is constructed and used as the moving platform for a 2R3T hybrid mechanism. This hybrid mechanism possesses high rotational performance and bifurcation, which can be applied to manufacture the 3D printers, the flight simulators, the multi-axis machine tools, etc.

(3) The proposed PMs, whose reachable rotating angles are larger than 180°, are more adequate for fast and low accuracy motions.

(4) The future research will focus on the kinematic analysis, the structural design of hybrid mechanisms with multidimensional non-bifurcated rotations and a properties comparison between the synthesized architectures.

Authors' Contributions
Y-FF was in charge of the whole trial; X-DJ wrote the manuscript; X-DJ, SG and H-BQ assisted with sampling and laboratory analyses. All authors read and approved the final manuscript.

Authors' Information
Xiao-Dong Jin, born in 1991, is currently a PhD candidate at *School of Mechanical, Electronic and Control Engineering, Beijing Jiaotong University, China*. He received his bachelor degree from *Huaqiao University, China*, in 2014. His research interests include spatial mechanism design and hybrid robots.

Yue-Fa Fang, born in 1958, is currently a professor and a PhD candidate supervisor at *School of Mechanical, Electronic and Control Engineering, Beijing Jiaotong University, China*. His main research interests include theory of mechanisms and parallel robots.

Sheng Guo, born in 1972, is currently a professor and a PhD candidate supervisor at *School of Mechanical, Electronic and Control Engineering, Beijing Jiaotong University, China*. His main research interests include spatial mechanism design and parallel robots.

Hai-Bo Qu, born in 1983, is currently a lecturer at *Robotics Institute, Beijing Jiaotong University*. He received his PhD from *Beijing Jiaotong University* in 2013. His research interests include robotics mechanism and mechanical design.

Publisher's Note

Jin *et al. Chin. J. Mech. Eng.* (2018) 31:61

Page 11 of 11

References

[1] R Clavel. DELTA: a fast robot with parallel geometry. *Proc. 18th International Symposium on Industrial Robot*, Lausanne, Switzerland, 1988. Berlin: Springer-Verlag, 1988: 91–100.

[2] O Piccin, B Bayle, B Maurin, et al. Kinematic modeling of a 5-DOF parallel mechanism for semi-spherical workspace. *Mechanism and Machine Theory*, 2009, 44(8): 1485–1496.

[3] F Gao, B B Peng, H Zhao, et al. A novel 5-DOF fully parallel kinematic machine tool. *The International Journal of Advanced Manufacturing Technology*, 2006, 31(1): 201–207.

[4] Y W Li, L M Wang, J F Liu, et al. Applicability and generality of the modified Grübler-Kutzbach criterion. *Chinese Journal of Mechanical Engineering*, 2013, 26(2): 257–263.

[5] H B Qu, Y F Fang, S Guo. Theory of degrees of freedom for parallel mechanisms with three spherical joints and its Applications. *Chinese Journal of Mechanical Engineering*, 2015, 28(4): 737–746.

[6] C C Lee, J M Hervé. Translational parallel manipulators with doubly planar limbs. *Mechanism and Machine Theory*, 2006, 24(4): 433–455.

[7] C C Lee, J M Hervé. Parallel mechanisms generating 3-DOF finite translation and (2 or 1)-DOF infinitesimal rotation. *Mechanism and Machine Theory*, 2012, 51(5): 185–195.

[8] W Ye, Y F Fang, S Guo, et al. Design of reconfigurable parallel mechanisms with discontinuously movable mechanism. *Journal of Mechanical Engineering*, 2015, 51(13): 137–143. (**in Chinese**)

[9] G Gogu. *Structural synthesis of parallel robots: part 2: translational topologies with two and three degrees of freedom*. New York: Springer, 2009.

[10] X J Liu, J Kim. A new spatial three-DOF parallel manipulator with high rotational capability. *IEEE/ASME Transactions on Mechatronics*, 2005, 10(5): 502–512.

[11] J Kim, F C Park, J M Lee. A new parallel mechanism machine tool capable of five-face machining. *CIPP Annals – Manufacturing Technology*, 1999, 48(1): 337–340.

[12] J Kim, J C Hwang, S K Jin, et al. Eclipse II: a new parallel mechanism enabling continuous 360–degree spinning plus three-axis translational motions. *IEEE Transactions on Robotics and Automation*, 2002, 18(3): 367–373.

[13] D S Kang, T W Seo, Y H Yoon, et al. A micro-positioning parallel mechanism platform with 100-degree tilting capability. *CIPP Annals – Manufacturing Technology*, 2006, 55(1): 377–380.

[14] F Pierrot, V Nabat, O Company, et al. Optimal design of a 4-DOF parallel manipulator: from academia to industry. *IEEE Transactions on Robotics*, 2009, 25(2): 213–224.

[15] F Pierrot, O Company. H4: a new family of 4-dof parallel robots. *Proceedings of IEEE/ASME International Conference on Advanced Intelligent Mechatronics*, Atlanta, USA, 1999: 508–513.

[16] O Company, S Krut, F Pierrot. Internal singularity analysis of a class of lower mobility parallel manipulators with articulated traveling plate. *IEEE Transactions on Robotics and Automation*, 2006, 22(1): 1–11.

[17] S Krut, O Company, M Benoit, et al. I4: a new parallel mechanism for scara motions. *Proceedings of IEEE International Conference on Robotics & Automation*, Taipei, Taiwan, China, 2003: 1875–1880.

[18] S Krut, V Nabat, O Company, et al. A high-speed parallel robot for scara motions. *Proceedings of IEEE International Conference on Robotics and Automation*, New Orleans, USA, 2004: 4109–4115.

[19] S Krut, O Company, C Corradini, et al. Evalution of a 4-degree of freedom parallel manipulator stiffness. *Proceedings of the 11th World Congress in Mechanism and Machine Science*, Tianjin, China, August 18-21, 2003. Beijing: China Machinery Press, 2003: 1857–1861.

[20] S Guo, Y F Fang, H B Qu. Type synthesis of 4-DOF nonoverconstrained parallel mechanisms based on screw theory. *Robotica*, 2012, 30(01): 31–37.

[21] S Guo, W Ye, H B Qu, et al. A serial of novel four degrees of freedom parallel mechanisms with large rotational workspace. *Robotica*, 2016, 34(04): 764–776.

[22] C Z Wang, Y F Fang, S Guo, et al. Design and analysis of 3R2T and 3R3T parallel mechanisms with high rotational capability. *Journal of Mechanisms and Robotica*, 2016, 8(4): 1–10.

[23] K Oh, X J Liu, D S Kang, et al. Optimal design of a micro parallel positioning platform, Part I: Kinematic analysis. *Robotica*, 2004, 22(6): 599–609.

[24] K Oh, X J Liu, D S Kang, et al. Optimal design of a micro parallel positioning platform, Part II: Real machine design. *Robotica*, 2005, 23(1): 109–122.

[25] X J Liu, J S Wang, G Pritschow. A new family of spatial 3-DOF fully-parallel manipulators with high rotational capability. *Mechanism and Machine Theory*, 2005, 40(4): 475–494.

[26] Q C Li, Q H Chen, C Y Wu. Geometrical distribution of rotational axes of 3-[P][S] parallel mechanisms. *Mechanism and Machine Theory*, 2013, 65(7): 46–57.

[27] J M Hervé. Analysestructurelle des mécanismes par groupe des déplacements. *Mechanism and Machine Theory*, 1978, 13(4): 437–450.

[28] C C Lee, J M Hervé. Type synthesis of primitive Schoenflies-motion generator. *Mechanism and Machine Theory*, 2009, 44(10): 1980–1997.

[29] S Refaat, J M Hervé, S Nahavandi, et al. Asymmetrical three-DOFs rotational-translational parallel-kinematics mechanisms based on Lie group theory. *European Journal of Mechanics A/Solids*, 2006, 25(3): 550–558.

[30] J M Hervé. The Lie group of rigid body displacements, a fundamental tool for mechanism design. *Mechanism and Machine Theory*, 1999, 34(5): 719–730.

[31] Q C Li, Z Huang, J M Hervé. Displacement manifold method for type synthesis of lower-mobility parallel mechanisms. *Science in China Ser. E Engineering & Materials Science*, 2004, 47(6): 641–650.

[32] J J Yu, J S Dai, S S Bi, et al. Type synthesis of a class of spatial lower-mobility parallel mechanisms with orthogonal arrangement based on Lie group enumeration. *SCIENCE CHINA Technological Sciences*, 2010, 53(2): 388–404.

[33] H Sun, Z M Chen, W J Ge. *Theory of machines and mechanisms*. Beijing: Higher Education Press, 2006. (**in Chinese**)